ELSEVIER

Ceramics International 32 (2006) 263–270

CERAMICS INTERNATIONAL

www.elsevier.com/locate/ceramint

Effect of thermal exposure on hardness and Young's modulus of EB-PVD yttria-partially-stabilized zirconia thermal barrier coatings

Shuqi Guo [a,*], Yutaka Kagawa [a,b]

[a] *Institute of Industrial Science, The University of Tokyo, 4-6-1 Komaba, Meguro-ku, Tokyo 153-8505, Japan*
[b] *Department of Materials Engineering, The University of Tokyo, 7-3-1 Hongo, Bunkyu-ku, Tokyo 113-8586, Japan*

Received 21 December 2004; received in revised form 4 January 2005; accepted 30 January 2005
Available online 26 April 2005

Abstract

The effect of thermal exposure on hardness and Young's modulus of 4.0 mol% Y_2O_3-partially-stabilized ZrO_2 coating material deposited by an electron beam physical vapor deposition has been investigated after exposure at 1200 °C and 1400 °C in air for up to 100 h, using an ultra-micro-indentation technique. The indentation tests were carried out with loading rate of 0.88 mN/s and holding time of 20 s at the maximum load of 50 mN. Before and after thermal exposure, the microstructure of the coating was characterized using scanning electron microscopy. Before thermal exposure, the coating showed a typical columnar structure. After thermal exposure, however, the columnar structure degraded and the degradation depended on exposure temperature and time. The hardness and Young's modulus were higher on the plan-section than on the cross-section before and after thermal exposure. The hardness and Young's modulus on both sections significantly increased after thermal exposure. The increases depended on exposure temperature and time, as a result of the sintering effect.

Keywords: C. Hardness; Young's modulus; EB-PVD TBC; Indentation; Thermal exposure

1. Introduction

Thermal barrier coatings (TBCs) have been used for almost three decades to extend the life of combustors and augmentors and, more recently, stationary turbine components [1,2]. Among them, air-plasma-sprayed (APS) and electron beam physical-vapor-deposited (EB-PVD) yttria-partially-stabilized zirconia TBCs have widely been studied in recent years because of their potential possibilities to substantially extend turbine lives and/or improve engine efficiencies [2–6], resulting from surface catalytic and emissivity effect of the ZrO_2 layer on combustion zone components. In particular EB-PVD TBCs have a longer service life compared to APS TBCs [6–8]. This superior performance of EB-PVD TBCs is due to their columnar microstructure, which exhibits very high levels of stress compliance [9,10], as a result of prevention of the individual columns of this columnar structure from the build-up of tensile stresses and from the match of the coefficient of thermal expansion differences between the TBCs and the base metal. To understand the full potential performance benefits offered by the TBCs, on the other hand, it is necessary quantitatively evaluating its mechanical properties.

Hardness and Young's modulus are the two essential mechanical properties of the TBCs, and they are measured and evaluated using various techniques [10–14]. These measurements [10–14] showed that hardness and Young's modulus were closely linked to process parameters, microstructure and surface roughness. Early studies [12,13] in APS TBC have showed that the Young's modulus was orientation specific, with higher modulus on the cross-section than on the plan-section. Furthermore, Young's modulus of the APS TBCs increased after thermal exposure between 1000 °C and 1400 °C for 100 h [13,14]. This increase depended on exposure temperature and time as well as on the measured section sides [13,14]. For the EB-PVD TBCs, however, hardness and Young's modulus on the cross-section and the plan-section and the effect of thermal exposure are little

* Corresponding author. Present address: Composites Group, National Institute for Materials Science, 1-2-1 Sengen, Tsukuba, Ibaraki 305-0047, Japan. Tel.: +81 29 859 2223; fax: +81 29 859 2401.
E-mail address: guo.shuqi@nims.go.jp (S. Guo).

0272-8842/$30.00
doi:10.1016/j.ceramint.2005.01.018

known. Therefore, it is required for the EB-PVD TBCs material to measure hardness and Young's modulus on the cross-section and plan-section before and after thermal exposure at elevated temperature. This study presents experimental results of hardness and Young's modulus on the cross-section and the plan-section of an EB-PVD yttria-partially-stabilized zirconia coating before and after thermal exposure at 1200 °C and 1400 °C in air for up to 100 h.

2. Experimental procedure

2.1. Specimen preparation

The material used in this study was a 4.0 mol% Y_2O_3-partially-stabilized ZrO_2 coating material, which was deposited by an electron beam physical vapor deposition (EB-PVD) onto a MA738LC nickel-based supperalloy substrate. The material was supplied by JFCC (Japan Fine Ceramic Center, Nagoya, Japan). Typically, the obtained coat was approximate 500 μm in thick. Before measurement, all specimens were polished with diamond paste up to 0.5 μm through a conventional metallographical process to eliminate influence of surface roughness on the measurement. Finally, the obtained polished coat specimens were about 200 μm in thick. To learn the effect of thermal exposure on hardness and Young's modulus, the polished specimens were thermally exposed at 1200 °C and 1400 °C in air for 25 h and 100 h in an electron furnace (S-73401, Hallstahammar, Sweden). The heating rate was 10 °C/min and the furnace cooling was used to cool the exposed specimens to room temperature. Before and after thermal exposure, the microstructures of the plan-section and the cross-section of the specimens were characterized by scanning electron microscopy (SEM), respectively.

2.2. Ultra-micro-indentation test

The ultra-micro-indentation tests were performed using a dynamic ultramicrohardness tester instrument (DUH-W201S, Shimadzu Corporation, Kyoto, Japan), with a displacement resolution of 1 nm and a force resolution of 0.2 μN. The polished specimen was affixed to a thick copper metal plate and then it was fixed in the table of the instrument. A microscope allowed the user to pinpoint the position at which an indent is to be made. Indents were performed on the cross-section and the plan-section of the specimen. The indentation tests were performed at loading rate of 0.88 mN/s, with a hold period duration of 20 s at the maximum load of 50 mN. The detailed measuring process has been reported elsewhere [15]. A minimum of 20 indentations were made for each measurement.

2.3. Hardness and Young's modulus determination

The hardness, H, is defined as the mean pressure under the indenter. With this definition, the hardness is calculated as the maximum applied load during indentation test, P_{max}, divided by the projection area, A_C, of contact between the indenter and the sample as follows

$$H = \frac{P_{max}}{A_C} \tag{1}$$

The projection contact area, A_C, is an indenter shape function at the contact depth, h_C. For an ideal pyramidal geometry case, the area function, A_C, is given by [16]:

$$A_C \approx 24.5 h_C^2 \tag{2}$$

The contact depth, h_C, immediately before unloading can be directly estimated from the load–displacement data and is given by [17]:

$$h_C = h_{max} - \varepsilon \frac{P_{max}}{S} \tag{3}$$

where ε is the geometric constant and the value $\varepsilon = 0.72$ is generally used [17] for a conical or pyramidal indenter, S is the experimentally measured stiffness of the upper portion of the unloading data (i.e., slope of the unloading curve) and is given by:

$$S = \frac{dP}{dh} \tag{4}$$

Young's modulus, on the other hand, is determined in the case of assuming that the area in contact remains constant during initial unloading. The relationship between load and displacement on initial unloading is related to the stiffness of the sample and the indenter, and to the contact area between the sample and the indenter, and is given by [18]:

$$E_r = \frac{1}{2\beta h_C}\sqrt{\frac{\pi}{24.5}}\left(\frac{dP}{dh}\right) \tag{5}$$

$$\frac{1}{E_r} = \frac{1-\nu^2}{E} + \frac{1-\nu_i^2}{E_i} \tag{6}$$

where β is a constant which depends on the geometry of the indenter ($\beta = 1.011$ for a Vickers indenter [19]), E_r is the reduced modulus, E and ν are the Young's modulus and Poisson's ratio for the sample, and E_i and ν_i are the same parameters for the indenter. The reduced modulus, E_r, is obtained from the slop of initial unloading curve and the contact depth, h_C, determined by Eq. (3). Poisson's ratio for the sample was assumed to be 0.23 [20] and the elastic properties of the diamond indenter used in this study were $E_i = 1141$ GPa and $\nu_i = 0.07$ [21].

3. Results

3.1. Microstructural characterizations

Fig. 1 shows SEM micrographs of the cross-section for the EB-PVD TBC before and after thermal exposure. For the as-received EB-PVD TBC (Fig. 1(a)), the typical columnar structure is observed. For the exposed EB-PVD TBC

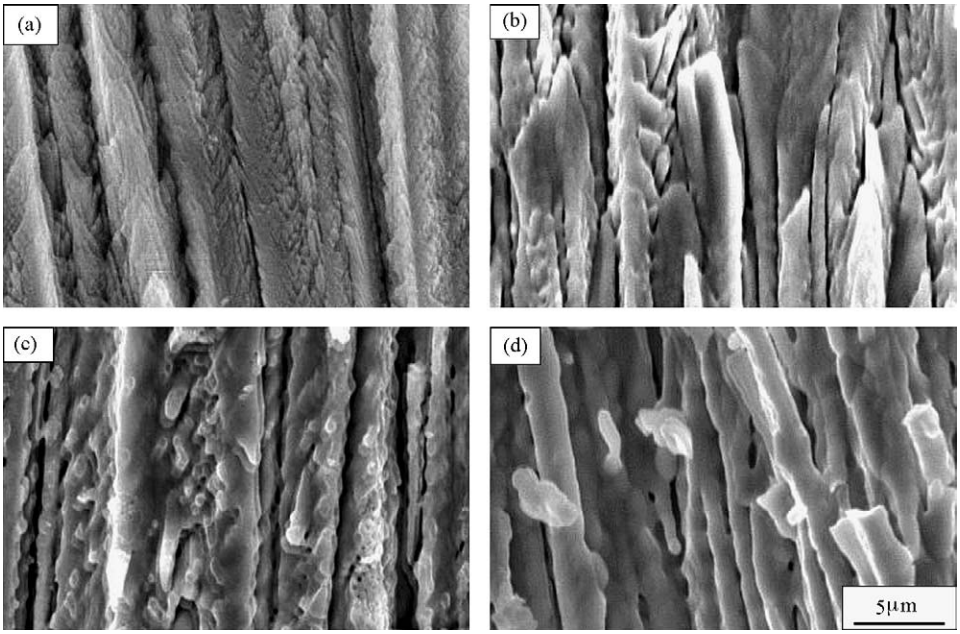

Fig. 1. SEM micrographs of the cross-section of the EB-PVD TBC for (a) as-received and exposed at (b) 1200 °C, 100 h; (c) 1400 °C, 25 h; and (d) 1400 °C, 100 h.

(Fig. 1(b)–(d)), however, the columnar structure degrades and the feather-like microstructure is reduced, as a result of sintering effect during thermal exposure. This degradation depends on exposure temperature and time. After 100 h exposure at 1200 °C (Fig. 1(b)), the individual columns are still observed, but the feather-like microstructure columns partially disappear. After exposure at 1400 °C (Fig. 1(c) and (d)), the columnar structure significantly degrades, in particular after 100 h exposure only trace amounts of individual columns are present and the feather-like microstructure almost disappears (Fig. 1(d)).

The sintering behavior of the EB-PVD TBC during thermal exposure is also observed on the polished top surface morphologies. Fig. 2 shows the typical SEM micrographs of the top surface of the polished EB-PVD TBC before and after thermal exposure. Before thermal exposure (Fig. 2(a)), the intercolumnar cracks are clearly observed, showing the presence of the individual columns.

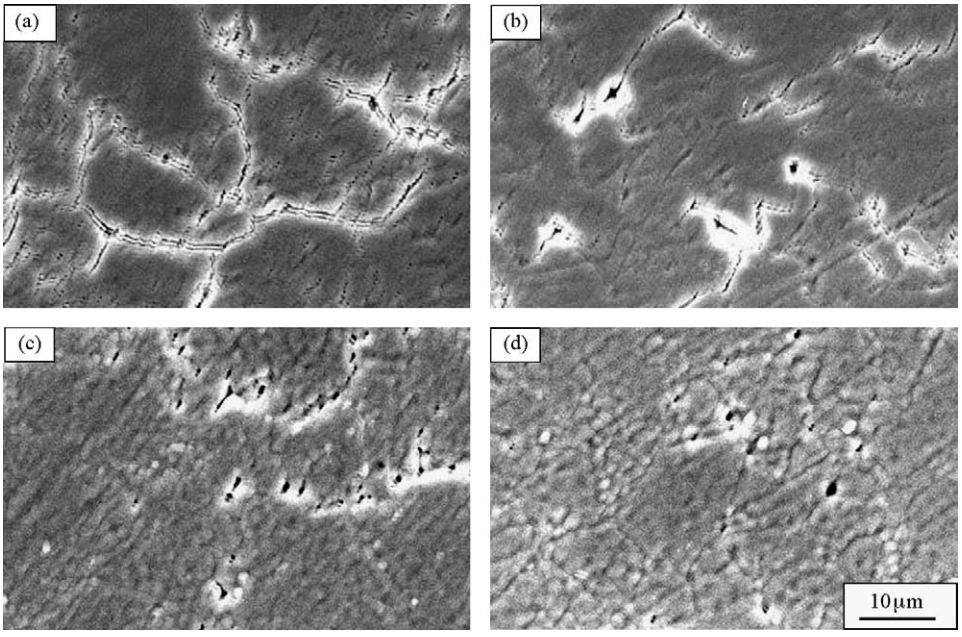

Fig. 2. SEM micrographs of the polished top surface morphologies of the EB-PVD TBC for (a) as-received and exposed at (b) 1200 °C, 100 h; (c) 1400 °C, 25 h; and (d) 1400 °C, 100 h.

After thermal exposure (Fig. 2(b)–(d)), the top surface morphologies change significantly and the previous clear columnar structural characterization partially and/or completely disappear, showing a sintering behavior during thermal exposure. In particular after exposure at 1400 °C the TBC is substantially sintered without the trace of the intercolumnar cracks, a few of pores are observed on the sintered surface instead of these cracks (Fig. 2(c) and (d)).

3.2. Indentation experimental

3.2.1. Load–displacement curves

In Fig. 3 typical indentation load–displacement profile curves obtained on the cross-section and the plan-section of the EB-PVD TBC before and after thermal exposure are presented. It is found that the load–displacement curves depended on thermal exposure temperature and time. This dependence of the cross-section differed with that of the plan-section. After thermal exposure, the penetration depth of indenter decreases, in particular for the cross-section the depth significantly decreases (Fig. 3(a)). In addition, the differences in the indenter penetration depths between the cross-section and the plan-section are larger for the as-received specimen than for the thermal exposed specimens. These differences decrease with increasing thermal exposure temperature and time. After 100 h exposure at 1400 °C, the differences almost are not observed.

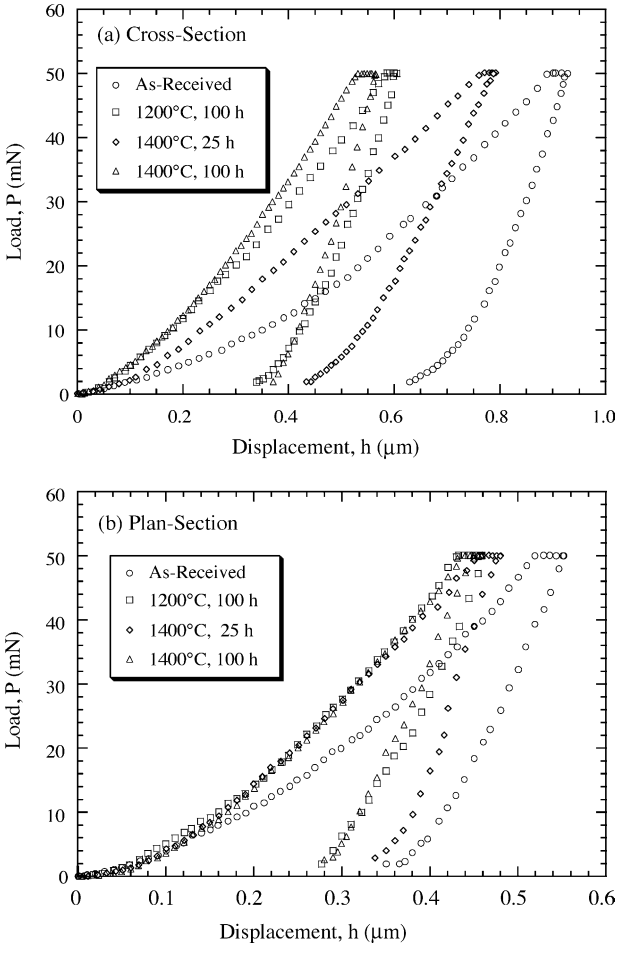

Fig. 3. Typical load–displacement curves of the EB-PVD TBC for the (a) cross-section and (b) plan-section before and after thermal exposure.

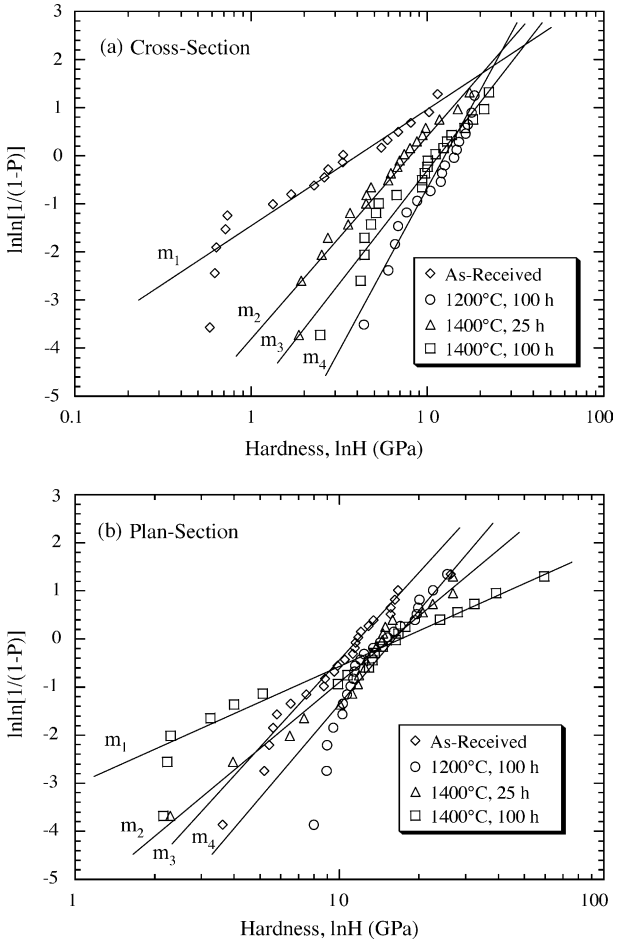

Fig. 4. Weibull hardness plots of the EB-PVD TBC for the (a) cross-section and (b) plan-section before and after thermal exposure.

3.2.2. Hardness

Fig. 4 shows Weibull plots of the hardness measured on the cross-section and the plan-section for the EB-PVD TBC before and after thermal exposure. In these plots, ln ln [1/(1 − P)] is displayed as a function of ln H. Where 1 − P is the probability that a measured value is lower than or equal to the measured value at the observed point for each measurement point. The obtained hardness data have been sorted in ascending order and a corresponding probability, $P = (i - 0.5)/N$, assigned to each hardness value, based on rank statistics. Here, i is the rank and N is the total number of measured hardness data. The straight lines in the Fig. 4 were determined by least-squares regression. The mean hardness values and Weibull moduli were determined using the two-parameter Weibull distribution [22]. The distinct Weibull distribution of the hardness is observed for the curves obtained on the cross-section and the plan-section before and after thermal exposure. This difference depends on

Table 1
Measured average hardness and Weibull modulus

Samples	Cross-section		Plan-section	
	H (GPa)	m_h	H (GPa)	m_h
As-received	3.8	1.1	1.1	2.7
1200 °C, 100 h	9.5	2.9	14.1	2.8
1400 °C, 25 h	6.8	1.8	1.8	1.9
1400 °C, 100 h	10.2	2.1	16.4	1.1

thermal exposure temperature and time. For the cross-section, Weibull curves obtained are shifted to the high values after thermal exposure (Fig. 4(a)). For the plan-section, this behavior is also observed, however, some data are lower for the as-received sample than the samples exposed at 1400 °C for 100 h (Fig. 4(b)).

Table 1 lists the average hardness and obtained Weibull modulus measured on the cross-section and the plan-section of the EB-PVD TBC before and after thermal exposure. It is found that the hardness of the plan-section is larger by a factor of ∼2 than that of the cross-section for the as-received EB-PVD TBC. After thermal exposure, the hardness significantly increases and this increase is larger on the cross-section than on the plan-section. On the other hand, Weibull modulus of the cross-section substantially increases after thermal exposure. For the plan-section, Weibull modulus slightly increases after 100 h exposure at 1200 °C, however, Weibull modulus decreases after exposure 1400 °C. In particular, after 100 h exposure, the modulus significantly decreases compared with the as-received sample.

Fig. 5 shows the effect of thermal exposure temperature and time on the hardness of the cross-section and the plan-section of the EB-PVD TBC. For the cross-section, the average hardness value increased from 3.8 GPa before thermal exposure to 9.5 GPa after 100 h of exposure at 1200 °C, 6.8 GPa and 10.2 GPa after exposure at 1400 °C for 25 h and 100 h, respectively, for gains of approximately 150%, 80% and 170%. For the plan-section, on the other hand, the average hardness increased from 10.9 GPa to 14.1 GPa after 100 h of exposure at 1200 °C, 13.7 GPa and 16.4 GPa after exposure at 1400 °C for 25 h and 100 h and it increased by about 30%, 26% and 50%, respectively.

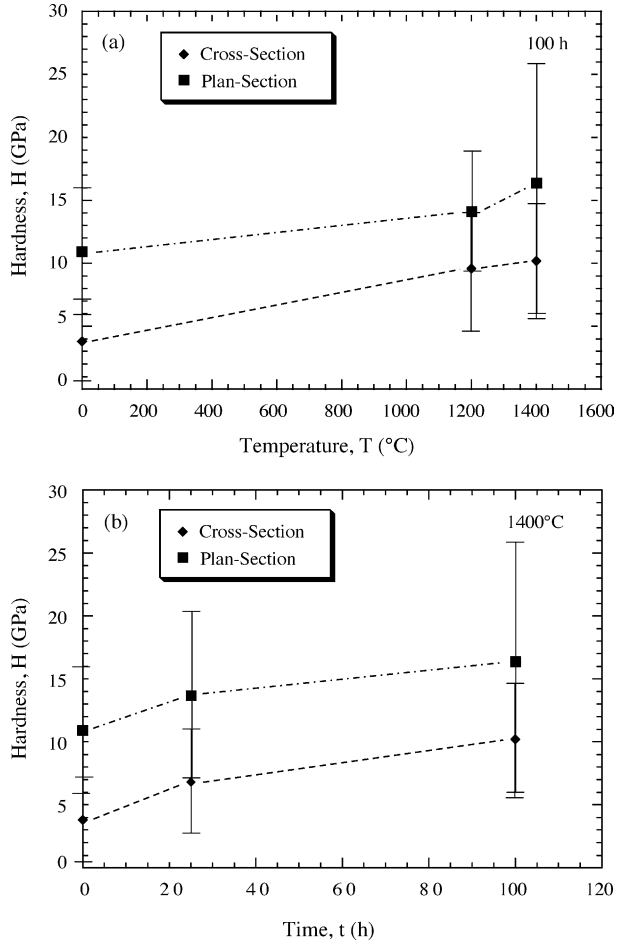

Fig. 5. Effects of (a) thermal exposure temperature and (b) time on the hardness measured on the cross-section and the plan-section for the EB-PVD TBC.

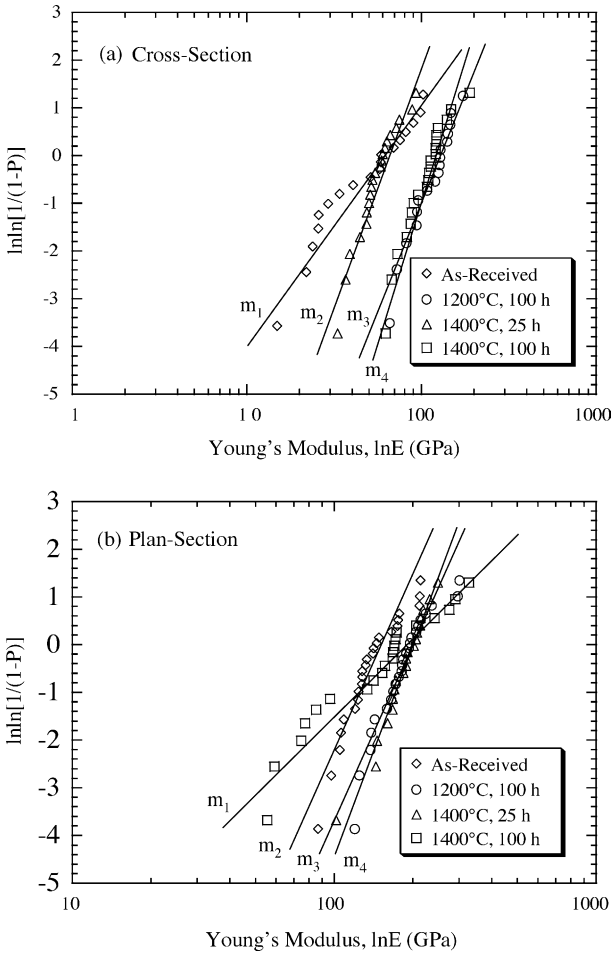

Fig. 6. Weibull Young's modulus plots of the EB-PVD TBC for the (a) cross-section and (b) plan-section before and after thermal exposure.

3.2.3. Young's modulus

Fig. 6 shows Weibull plots of the measured Young's modulus values of the cross-section and the plan-section for the EB-PVD TBC before and after thermal exposure. The calculation method of the Weibull statistic is the same as that described before. The Young's modulus obtained on both sections shows similar Weibull distributions to the hardness (Fig. 4). Before thermal exposure, the Weibull curves of Young's modulus are in lower value ranges for both sections. After thermal exposure, the Weibull curves are shifted to higher values ranges. For the cross-section, after 100 h exposure at 1200 °C and 1400 °C, Weibull distributions are the nearly same and are in the highest values. For the plan-section, Weibull distribution curves are the nearly same for the samples exposed at 1200 °C for 100 h and at 1400 °C for 25 h, however, the distinct Weibull distribution curve was recognized after 100 h exposure at 1400 °C.

Table 2 lists the average Young's modulus and Weibull modulus obtained on the cross-section and the plan-section for the EB-PVD TBC before and after thermal exposure. Young's modulus and Weibull modulus of both sections are larger after thermal exposure than before thermal exposure. Furthermore, Young's modulus is substantially lower for the cross-section than for the plan-section. Although this difference increases after 25 h exposure at 1400 °C, it is significantly reduces after 100 h exposure at 1200 °C and 1400 °C. On the other hand, Weibull modulus is lower for the cross-section than for the plan-section before and after thermal exposure, in particular for the as-received sample this difference is the highest. One exception is larger Weibull modulus for the cross-section than for the plan-section after 100 h exposure at 1400 °C.

Fig. 7 shows the effect of thermal exposure on Young's modulus of the cross-section and the plan-section for the EB-PVD TBC. For the cross-section, the average value of Young's modulus substantially increases from 53.3 GPa before thermal exposure to 104.1 GPa after 100 h exposure at 1200 °C, 57.4 GPa and 108.8 GPa after exposure at 1400 °C for 25 h and 100 h, respectively for gains of approximately 95%, 8% and 104%. For the plan-section, the average value of Young's modulus increases from 142.8 GPa to 187.8 GPa after 100 h exposure at 1200 °C, 185.9 GPa and 161.1 GPa after exposure at 1400 °C for 25 h and 100 h and it increases by about 32%, 31% and 13%, respectively.

Table 2
Measured average Young's modulus and Weibull modulus

Samples	Cross-section		Plan-section	
	E (GPa)	m_e	E (GPa)	m_e
As-received	53.3	2.2	142.8	5.4
1200 °C, 100 h	104.1	4.8	187.8	5.6
1400 °C, 25 h	57.4	4.6	185.9	6.4
1400 °C, 100 h	108.8	3.9	161.1	2.4

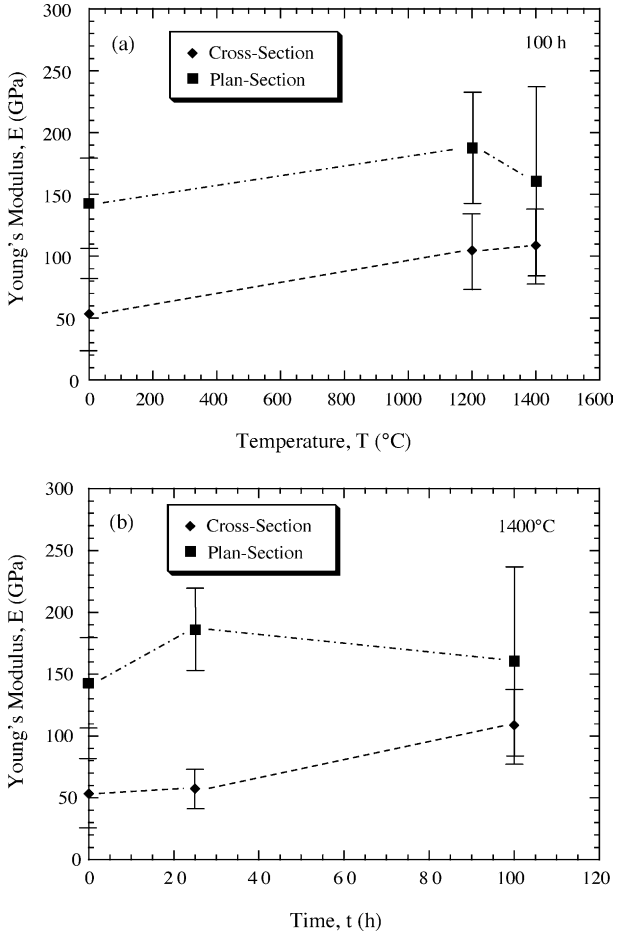

Fig. 7. Effects of (a) thermal exposure temperature and (b) time on the Young's modulus measured on the cross-section and the plan-section for the EB-PVD TBC.

4. Discussion

4.1. Microstructural evolution

SEM observations of the polished top surfaces and the cross-sections of the as-received and exposed EB-PVD TBC show that the columnar structure degraded after thermal exposure (Figs. 1 and 2), dependent on exposure temperature and time. The degradation in the columnar structure due to exposure at high temperature is closely associated with sintering behavior of TBC during thermal exposure. The sintering effect results in disappearance of the feather-like microstructure between the individual columns, densification, and shrinkage of the EB-PVD TBC after thermal exposure. This effect is closely linked with thermal temperature, time as well as with composition of coating material. An early study [23] in a plasma-sprayed TBC indicated that the significant shrinkage strains due to the sintering were detected above the temperature of 900 °C. Furthermore, the sintering rates at the isothermal stages change with time especially at the early sintering time period; faster shrinkage rates are initially observed, and

relatively constant rates are observed for longer sintering time. Thus, it is reasonable to conclude that after thermal exposure, the degradation in the columnar structure observed in the studied TBC with exposure temperature and time are attributable to the different sintering rates. In addition, after thermal exposure, it is found that the permanent curvature of TBC was present and it was more serious with exposure temperature and time. This suggests that the shrinkage rates due to the sintering were different at the top and the bottom of TBC. This seems to be associated with the finer column grains at the bottom than at the top [24] because the fine grains resulted in a larger shrinkage than the coarse grains during the sintering.

4.2. Effect of thermal exposure on hardness and Young's modulus

The hardness and Young's modulus measured on the plan-section were always larger than those on the cross-section for the as-received and the exposed specimens (Figs. 5 and 7). This indicated that an anisotropic was present in the hardness and Young's modulus for the studied material. Early studies in plasma-sprayed TBC have reported the anisotropic in Young's modulus [12,13]. Wallace and Llavsky [13] showed Young's modulus measured on the cross-section was larger by a factor of ~1.3 than that on the plan-section. This is attributed to the high density of planar defects that are nearly parallel to the substrate [12,13]. In this study, the pores and the planar crack-like flaws are present between the individual columns of the EB-PVD TBC (Fig. 1). These planar defects are higher on the cross-section than on the plan-section (Figs. 1 and 2). Thus, hardness and Young's modulus measured on the cross-section are lower than those on the plan-section because they depended strongly on the degree of contact between the single columns [10].

On the other hand, it is found that the hardness and Young's modulus increased substantially after exposure at 1200 °C and 1400 °C (Figs. 5 and 7). The magnitude of the increases depends on exposure temperature and time. Generally, the hardness and Young's modulus increase with increasing exposure temperature and time (Figs. 5 and 7). One exception is the decrease of Young's modulus for the plan-section after exposure at 1400 °C for 100 h compared to those after exposure at 1200 °C for 100 h and at 1400 °C for 25 h. This seems to be attributed to the curvature of TBC after thermal exposure, which induced a tensile stress on the top surface of the plan-section. In addition, this curvature of TBC results in larger scatter of hardness and Young's modulus values measured on the plan-section than on the cross-section after thermal exposure (Tables 1 and 2). The increase in Young's modulus due to exposure to high temperature is documented in the literature. Significantly increased Young's modulus has been reported for plasma-sprayed TBC after exposure between 1000 °C and 1400 °C for 100 h in air [13,14]. Kaden et al. [25] showed that the Young's modulus of EB-PVD TBCs increased by about 35% after exposure at 1000 °C for 100 h in air. This increase is attributable to more close contact between the single columns for EB-PVD TBC [8] and to improvement in bonding and coherence across the splat boundary for plasma-sprayed TBC [13,14], as a result of sintering effect. Similar sintering effects observed in the present study after exposure at both 1200 °C and 1400 °C in the period of 25–100 h for each instance (Figs. 1 and 2) contribute to a stiffer structure and thus should create a higher hardness and Young's modulus. Thus, it is reasonable to conclude that the increase in the measured hardness and Young's modulus is attributable to a more close contact between the single columns after thermal exposure, resulting from the sintering effect of EB-PVD TBC during the thermal exposure.

5. Conclusions

The microstructure, hardness and Young's modulus of an EB-PVD TBC have been examined before and after exposure at 1200 °C and 1400 °C in air for up to 100 h. The microstructure of the coating was characterized by using SEM. The hardness and Young's modulus were evaluated on the plan-section and the cross-section, using an ultra-micro-indentation technique. The effect of thermal exposure on these properties was discussed. The major results obtained are follows:

(1) Before thermal exposure, TBC showed a typical columnar structure with porosity defects between the individual columns. After thermal exposure, however, the columnar structure degraded, resulting in a close contact of columns as a result of sintering effect.
(2) The hardness and Young's modulus measured were higher on the plan-section than on the cross-section before and after thermal exposure.
(3) The hardness and Young's modulus measured on the plan-section and the cross-section increased significantly after thermal exposure. The increases in the hardness and Young's modulus were attributed to the sintering effect of the coating during the thermal exposure, dependent on exposure temperature and time.

Acknowledgments

This work was supported by New Energy and Industrial Technology Development Organization (NEDO) under "Nano-Coating Project". The first author (SQG) would also like to thank the NEDO for the fellowship.

References

[1] G.W. Goward, Progress in coatings for gas turbine airfoils, Surf. Coat. Technol. 108/109 (1998) 73–79.

[2] W. Beele, G. Marijnissen, A. van Lieshout, The evolution of thermal barrier coatings-status and upcoming solutions for today's key issues, Surf. Coat. Technol. 120/121 (1999) 61–67.
[3] M. Peters, C. Leyens, U. Schulz, W.A. Kaysser, EB-PVD thermal barrier coatings for aeroengines and gas turbines, Adv. Eng. Mater. 3 (4) (2001) 193–204.
[4] P.K. Wright, Influence of cyclic strain on life of a PVD TBC, Mater. Sci. Eng. A 245 (1998) 191–200.
[5] B.Z. Janos, E. Lugscheider, P. Remer, Effect of thermal aging on the erosion resistance of air plasma sprayed zirconia thermal barrier coating, Surf. Coat. Technol. 113 (1999) 278–285.
[6] E. Tzimas, H. Mullejans, S.D. Peteves, J. Bressers, W. Stamm, Failure of thermal barrier coating systems under cyclic thermomechanical loading, Acta Mater. 48 (2000) 4699–4707.
[7] D.J. Wortman, B.A. Nagaraj, E.C. Duderstadt, Thermal barrier coatings for gas turbine use, Mater. Sci. Eng. A 120 (1989) 433–440.
[8] C. Leyens, U. Schulz, B.A. Pint, I.G. Wright, Influence of electron beam physical vapor deposited thermal barrier coating microstructure on thermal barrier coating system performance under cyclic oxidation conditions, Surf. Coat. Technol. 120/121 (1999) 68–76.
[9] P. Scardi, M. Leoni, L. Bertini, L. Bertamini, Residual stress in partially-stabilised zirconia TBCs: experimental measurement and modelling, Surf. Coat. Technol. 94/95 (1997) 82–88.
[10] E. Lugscheider, K. Bobzin, S. Bärwulf, A. Etzkorn, Mechanical properties of EB-PVD thermal barrier coatings by nanoindentation, Surf. Coat. Technol. 138 (2001) 9–13.
[11] K. Duan, R.W. Steinbrech, Influence of sample deformation and porosity on mechanical properties by instrumental microindentation technique, J. Eur. Ceram. Soc. 18 (1998) 87–93.
[12] J.S. Wallace, J. Llavsky, Elastic modulus measurements in plasma sprayed deposits, J. Thermal Spray Technol. 7 (4) (1998) 521–526.
[13] S.Q. Guo, Y. Kagawa, Young's moduli of zirconia top-coat and thermally growth oxide in a plasma-sprayed thermal barrier coating system, Scripta Mater. 50 (2004) 1401–1406.
[14] J.A. Thompson, T.W. Clyne, The effect of heat treatment on the stiffness of zirconia top coats in plasma-sprayed TBCs, Acta Mater. 49 (2001) 1565–1575.
[15] S.Q. Guo, Y. Kagawa, Effect of loading rate and holding time on hardness and Young's modulus of EB-PVD thermal barrier coating, Surf. Coat. Technol. 182 (2004) 92–100.
[16] J.M. Antunes, A. Cavaleiro, L.F. Menezes, M.I. Simoes, J.V. Fernandes, Ultra-microhardness testing procedure with Vickers indenter, Surf. Coat. Technol. 149 (2002) 27–35.
[17] W.C. Oliver, G.M. Pharr, An improved technique for determining hardness and elastic modulus using load and displacement sensing indentation experiments, J. Mater. Res. 7 (6) (1992) 1564–1583.
[18] I.N. Sneddon, The relation between load and penetration in the axisymmetric boussinesq problem for punch of arbitrary profile, Int. J. Eng. Sci. 3 (1965) 47–57.
[19] R.B. King, Elastic analysis of some push problems for a layered medium, Int. J. Solids Struct. 23 (1987) 1657–1664.
[20] K.A. Khor, Y.W. Gu, Effect of residual stress on the performance of plasma sprayed functionally graded ZrO_2/NiCoCrAlY coatings, Mater. Sci. Eng. A 277 (2000) 64–76.
[21] G. Simmons, H. Wang, Single Crystal Elastic Constants and Calculated Aggregate Properties: A Handbook, MIT Press, Cambridge, MA, 1971.
[22] W. Weibull, A statistical distribution function of wide applicability, J. Appl. Mech. 18 (1951) 293–297.
[23] D. Zhu, R.A. Miller, Sintering and creep behavior of plasma-sprayed zirconia- and hafnia-based thermal barrier coatings, Surf. Coat. Technol. 108/109 (1998) 114–120.
[24] J.R. Nicholls, K.J. Lawson, A. Johnstone, D.S. Rickerby, Methods to reduce the thermal conductivity of EB-PVD TBCs, Surf. Coat. Technol. 151/152 (2002) 383–391.
[25] U. Kaden, C. Leyens, M. Peters, W.A. Kaysser, Werkstoffewoche 98, Vol. II, Werkstoffe für die Verkehrstechnik, Wiley-YCH, Weinheim, 1999, pp. 485–490.